Real-time Implementation of a Delay Compensation Block in the Power Plant Controller of a Renewable Energy Complex using MLPNN

Abhilash Sen
Dept. of Electrical Engineering,
Indian Institute of Technology Kanpur,
Kanpur, India.
abhilashsen0070@gmail.com

Swakshar Ray
Director,
RAY-D-US Renewable Pvt Ltd,
Kolkata, India.
swakshar@gmail.com

Ebin Mathew
Dept. of Electrical Engineering
Indian Institute of Technology Kanpur,
Kanpur, India.
ebincm@iitk.ac.in

***Abstract* -- The power plant controllers (PPC) generate the power commands for all the individual inverters, Wind turbine generators (WTGs) and Static var generators (SVGs) in a Renewable Energy (RE) complex. However, there are several delays involved in PPC sensing the grid voltage and the command actually reaching the inverters. These delays can cause oscillations in the system, mainly voltage and reactive power fluctuations. A delay-compensation mechanism that compensate the delay using a Multi-Layer Perceptron neural network (MLPNN) is presented in this paper. The MLPNN is equipped with a triggered online back-propagation (BP) training algorithm. A hardware-in-loop (HIL) validation is done through Real-Time Digital Simulator (RTDS), simulating the plant with PPC, and DSP F28379D implementing the MLPNN. The real-time results with PPC delay indicate QV oscillations and prolonged post-fault HVRT mode. When the MLPNN is enabled, it compensates the delay and dampens oscillations within 2-5s, depending on the instance of switching. It also improves post-fault conditions with a smooth transition to the pre-fault state. The method is validated using frequency domain-based system identification. The advantages of the proposed method are also compared with the existing classical methods.**

***Index Terms*--delay compensation, power plant controller, neural network, QV oscillations, triggered online training**

I. Introduction

The integration of renewable energy (RE) resources into power systems has increased significantly over the past two decades, transitioning from small-scale photovoltaic (PV) installations in distribution networks to large utility-scale RE complexes connected at the transmission level. In 2005, the global installed renewable energy capacity was approximately 160 GW, which increased to approximately 1437 GW by the end of 2020 [1]. This rapid growth from kilowatt to multi-megawatt-scale generation has introduced several operational and control challenges in power systems.

Utility-scale PV and wind installations, often ranging from 100 to 500 MW, are typically connected to isolated pooling stations. A notable example is the large-scale RE installations in Rajasthan, driven by its favorable geographical and climatic conditions. In many cases, these stations lack sufficient support from synchronous generators, resulting in weak grid conditions characterized by a low short-circuit strength.

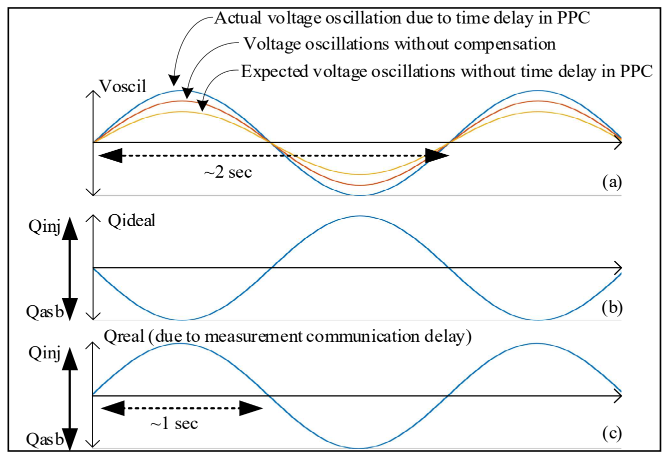

Fig. 1. Illustration of out-of-phase injection of reactive power due to PPC delay (a) Oscillatory component of Line-Line rms voltage at POI (0.1 p.u) (b) Required reactive power oscillation to damp voltage oscillations, (c) Actual reactive power injected due to PPC delay.

Another challenge arises from the need to coordinate a large number of inverter-based resources (IBRs) within a RE single plant. A typical RE plant may consist of hundreds of inverters with different power ratings supplied by multiple manufacturers. Therefore, the power plant controller (PPC) must ensure a coordinated dynamic response and power sharing among all inverters according to their respective ratings. Furthermore, grid codes require large RE plants to behave as a single controllable entity rather than an aggregation of independent inverters [2], [3]. These requirements include voltage regulation, reactive power support, and fault-ride-through capability at the point of interconnection (POI). To meet these requirements, a centralized PPC is used in RE plants.

Based on the operating modes and reference set points selected by the grid operator, the PPC acquires electrical quantities at the point of interconnection (POI) via a PQ meter and dispatches active and reactive power commands to individual inverter-based resources (IBRs) in proportion to their rated capacities. The commonly implemented reactive power control modes in PPCs include (i) fixed reactive power (Fixed-Q) mode, (ii) power factor control mode, (iii) voltage

979-8-3315-8138-1

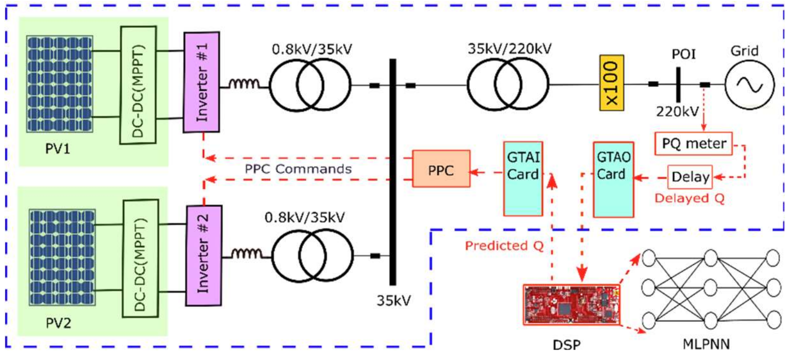

Fig. 2. Schematic representation of the entire system.

regulation mode, and (iv) Q–V droop control mode. Among these, the voltage regulation and Q–V droop modes provide dynamic voltage support by modulating the reactive power exchange between the RE plant and the grid [4].

Recent studies have highlighted stability concerns associated with power plant controllers (PPCs). In [5], the authors analyzed the impact of PPC dynamics on voltage and reactive power oscillations at the point of interconnection (POI). Field observations in India by the National Load Dispatch Centre (NLDC) since 2022 have further reported the occurrence of persistent Q–V oscillations in several large renewable energy (RE) plants, even in the absence of external disturbances [6]. Detailed analysis of phasor measurement unit (PMU) data from RE pooling stations revealed that these oscillations are closely associated with delays in PQ meter measurements, communication delays between the PQ meter and the PPC, and between the PQ meter and individual inverters, as well as nonuniform and slow inverter polling rates. These factors collectively lead to out-of-phase reactive power injection, as illustrated in Fig. 1 [5],[6].

There are multiple sources of delay in an RE power plant. It is reported that voltage and current measurement delays typically range from 20 ms to 50 ms [7]. In older installations, PQ meters often rely on slower communication channels, resulting in signal delays of 250 ms or more between the PQ meter and the PPC. In addition, individual inverters operate with different polling rates, typically ranging from 100 to 500 ms. The cumulative effect of these nonuniform and time-varying delays leads to uncoordinated reactive power injection and incorrect voltage support at the plant level. Neglecting these delays can significantly degrade the performance of PV plant control systems [8].

Most existing studies address the delay effects at the inverter or inverter-controller level rather than at the PPC. In [10], delays associated with digital control in power electronic converters were analyzed, and a graphical delay-compensation approach was proposed. A Smith-predictor-based method was presented in [11] to mitigate the delay effects in inverter control loops. In [12], a state observer–based delay compensation technique was introduced to compensate the delay. However, this approach imposed a relatively high computational burden on the controller. A neural network–based delay compensation scheme was proposed in [13], but it relies on offline training, making the model data-dependent and less adaptable to changing operating conditions. Moreover, implementing delay compensation at the inverter level is not practical for large RE plants, as they typically consist of hundreds of inverters.

This study proposes an online multilayer perceptron neural network (MLPNN)–based delay compensation strategy implemented at the PPC level. The proposed approach helps in the correct injection of reactive power signal by compensating for aggregate plant-level delays, thereby enabling coordinated voltage support and improving the dynamic performance of the RE plant.

II. System in Study

The renewable energy (RE) complex used in this study is shown in Fig. 2. It consists of a solar farm with two photovoltaic (PV) systems connected to the POI via a collector bus. Each PV system is equipped with an independent maximum power point tracking (MPPT)-based DC–DC boost converter, a two-level voltage source (VSI), an LC output filter, and a three-phase step-up transformer. The system ratings are summarized in Table I. The transformer arrangement steps up the voltage from 0.8 to 33 kV and subsequently from 33 to 220 kV for grid interconnection. The scaling of number of inverters is done in the transformer block.

A PQ meter installed at the point of interconnection (POI) measures the voltage and power quantities required for plant-level control. Based on these measurements and the reference points, the PPC computes the control references and dispatches active and reactive power commands to individual inverters. In this study, the PPC operates in the voltage regulation (V-regulation) control mode.

Table I. System parameters

Parameter	Value	Parameter	Value
System rating	300 MW	Irradiance	1000W/m^2
Solar PV	1.5 MW each	Switch Freq $_{Boost}$	2 kHz
Inverter Rating	1.8 MVA	No of Inverters	200
DC voltage	0.8 kV	L_{Boost}	250uH
Temperature	25 ºC	C_{DClink}	32000uF
$L_{Filter,}$ C_{Filter}	63uH, 1500uF	Switch Freq $_{inv}$	2 kHz
Grid voltage	220 kV	Grid SCR	6

III. Proposed Delay Compensation using MLPNN

The delay compensation block is inserted between the PQ meter output and the PPC input. The method uses a feedforward multi-layer perceptron neural network trained via triggered online training BP algorithm.

A. Multi-layer perceptron neural network (MLPNN)

The neural network structure used in the method is presented in Fig. 3. The network consists of a linear input layer with bias, one hidden layer with *tanh* activation function and linear output layer. The RTDS system provides the real-time Q data to the neural network model. The model takes *k* past sampled values of the Q, measured from PQ meter. An additional input of PPC Q command is also included so as to capture the closed-loop dynamics. As output, the model gives the Q predicted value, which compensates for the PQ meter delay. Let us consider the input to the neural network as a matrix u, then:

$$u = [Q_t, Q_{t-1}, Q_{t-2}, Q_{t-3}, Q_{t-4}, Q_{t-k+1}, Q_{cmd}] \tag{1}$$

Then the output can be calculated as (2)-(4):

$$g = w1\,.u + b1 \tag{2}$$

$$h = \tanh{(g)} \tag{3}$$

$$ypred = \ w2\,.h \tag{4}$$

The error L_{MSE} is calculated after next k sampled values arrive along with the actual value $yact$.

$$L_{MSE} = \frac{1}{2}(ypred - yact)^2 \tag{5}$$

Then, the gradients can be calculated as:

$$dw2 = -L_{MSE}\ .\ h' \tag{6}$$

$$dz2 = w2'\,.L_{MSE}\,.(1 - tanh^2 g) \tag{7}$$

$$dw1 = -dz2\ .\ u' \tag{8}$$

$$db1 = w2'\,.L_{MSE}\,.(1 - tanh^2 g) \tag{9}$$

Finally, the weights can be updated as follows:

$$w1 = w1 - alpha\,.dw1 \tag{10}$$

$$w2 = w2 - alpha.dw2 \tag{11}$$

$$b1 = b1 - alpha.db1 \tag{12}$$

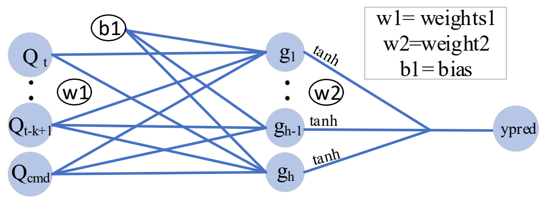

Fig. 3. MLPNN network structure.

B. Triggered Online Learning Algorithm

The network follows a triggered online learning with back-propagation-based weight updating. The algorithm has two main switches, S_1 for enabling/disabling MLPNN and S_2 for switching the learning rate between *alpha* and zero. Switch S_1 is controlled by the user, while S_2 is controlled internally, through a hysteresis band. The use of a hysteresis band on the test error prevents chattering and provides a stable output. As evident in Fig. 4, the testing process is continuous, whereas the training process is conditional. The weights are updated only when the test error goes above a predefined threshold. This is done to reduce the computational burden on the DSP.

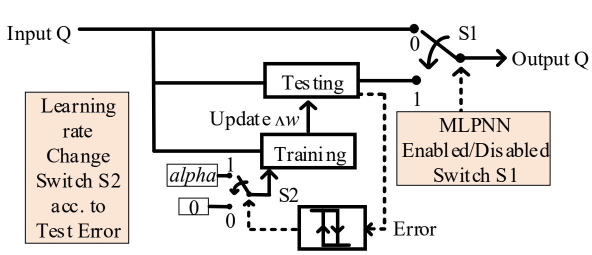

Fig. 4. Triggered online Training/Testing method

IV. HIL Results and Discussions

This section presents the hardware-in-the-loop (HIL)–based validation of the proposed delay-compensation method with the RE plant simulated in a real-time digital simulator (RTDS) and MLPNN algorithm implemented in a DSP TMS320F28379D. The overall system configuration is shown in Fig. 2, the triggered online training and testing algorithm is illustrated in Fig. 4, and the experimental setup is depicted in Fig. 5. The host desktop executes the photovoltaic (PV) system model in RTDS via the RSCAD FX interface, while the multi-layer perceptron neural network (MLPNN) is implemented on the DSP platform.

The MLPNN parameters are selected as follows: the number of inputs is 7 (6 past samples and Q_{cmd}), the number of hidden neurons h is 20, input delay window k is 6, and learning rate α/*alpha* is 0.01. The lower and upper hysteresis thresholds for the triggered training mechanism are set to 0.02 and 0.1, respectively. All results presented in this section are recorded in real time at intervals of 10 s using the RSCAD FX interface.

A. Operation without delay compensation

1) Steady-state normal condition with no delay

To establish baseline system performance, the system is first operated under steady-state conditions without any measurement delay, with the PPC operating in voltage regulation (V_{rms}) control mode. The results obtained are shown in Fig. 6. The reference values at the PPC, V_{rms} reference and P reference are fixed at 0.95pu and 0.4pu respectively. As observed, both the active power and RMS voltage at the point of interconnection (POI) accurately track their respective reference values. In this case, the measured and actual reactive power values are same at 0.9 p. u.

2) With a delay 0.25s in Q measured at POI

To demonstrate the impact of measurement delay, a delay of 0.25 s is introduced in the reactive power signal measured at the POI. The delay is applied at time 4.5s, as shown in Fig. 7. A sustained oscillations in the POI voltage with a dominant frequency of approximately 1.3 Hz and a peak-to-peak magnitude of about 0.02 pu is observed. The measured reactive power exhibits oscillations at the same frequency with a significantly larger amplitude of approximately 0.25 pu. Although active power also exhibits oscillatory behavior, its magnitude is small. It is worth noting that the V_{rms} oscillations and the Q measured (in red) are almost in-phase, denoting probable amplification of oscillations.

3) Three-phase fault with a delay 0.25s in Q measured

Fig. 8 shows the real-time result of 4 secs for a three-phase fault at the POI for 0.03s. The V_{rms} dips to 0.15pu and HVRT is followed after fault is cleared for a further 0.3s. The system returns to its oscillation state at 1sec

B. Operation with delay compensation (MLPNN enabled).

1) With a delay of 0.25s in Q measured

Fig. 9 shows the effect of the MLPNN on the PPC control. At 3s, the MLPNN predictor is activated. It is observed that the algorithm compensates the delays associated with the PQ meter-PPC-Inverter loop. The oscillations in V_{rms}, Q and P are damped and system settles to its stable initial values.

2) Increasing P_{ref} and V_{ref} and MLPNN enabled.

To verify the method while in normal operation, a step change in V_{rms} is introduced at 3s as shown in Fig. 10. Similarly, the active power reference P_{ref} is changed through the PPC controller from 0.4pu to 0.5pu as shown in Fig. 11. It is observed that in both cases effect of the delay is compensated and the Q responds instantly to the reference changes.

3) Three-phase fault with MLPNN enabled

A three-phase fault at the POI for 0.03s is introduced exactly at 0.6s. The differences observed while MLPNN is enabled are presented in Fig. 12. The V_{rms} dip is same for both cases, but the HVRT mode after the fault clearance disappears. It is thus inferred that the delay of 0.25 s was responsible for the initiation of the HVRT mode during post-fault recovery.

The frequency domain system identification was performed, with three different time-ranges for the fault cases as shown in Table 2. First time-range is 0s-3s when the MLPNN is disabled followed by the time which captures the transition after MLPNN is enabled, and finally, the complete time-range capturing the overall event. Two cases are taken based on different instances of MLPNN switching.

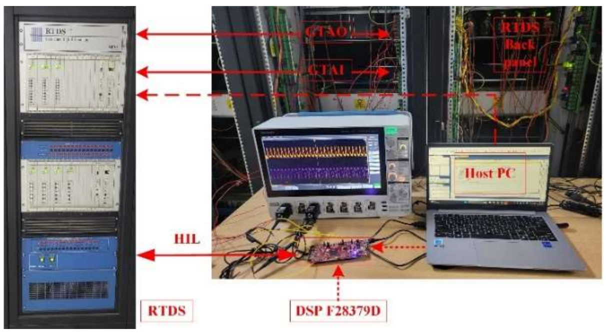

Fig. 5. Experimental set-up.

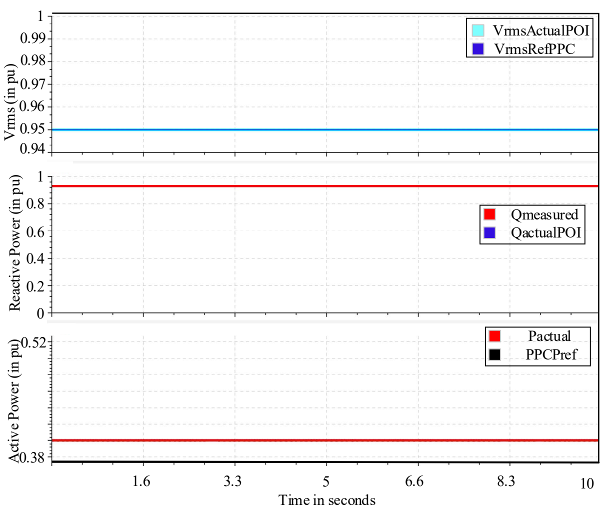

Fig. 6. Normal operation showing Vrms, Q and P, MLPNN disabled.

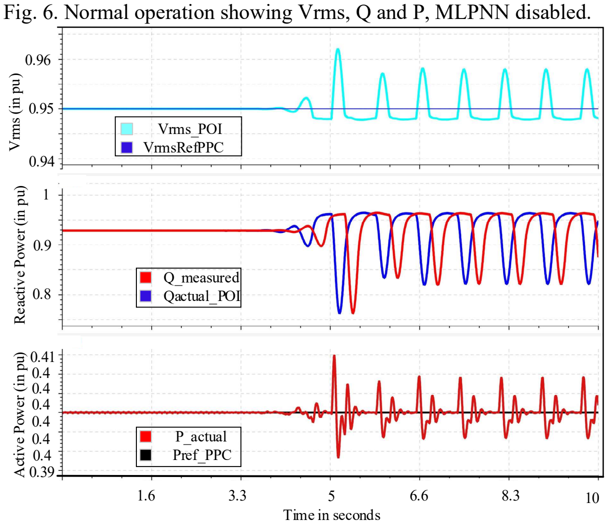

Fig. 7. A delay of 0.25s is introduced with MLPNN disabled.

The frequency domain analysis shows that there is a 1.31 Hz lightly damped oscillations from 0-3s range. After the MLPNN estimator is turned on, i.e., 2s-5s, zeta or damping ratio is 0.87 for case 1 and unity for case 2, indicating strongly damped system behaviour.

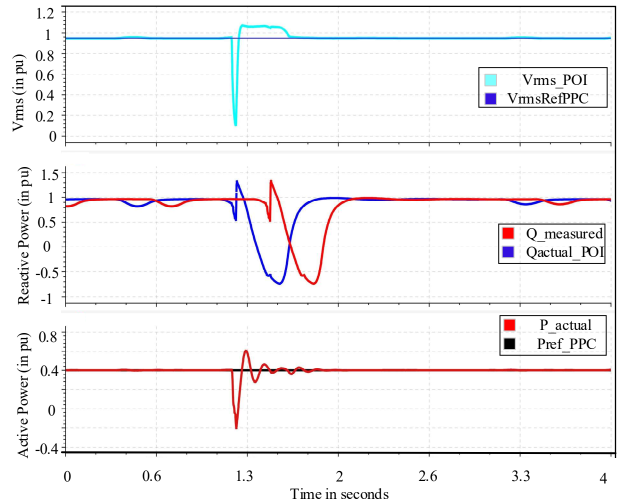

Fig. 8. A three-phase fault introduced at POI while MLPNN disabled.

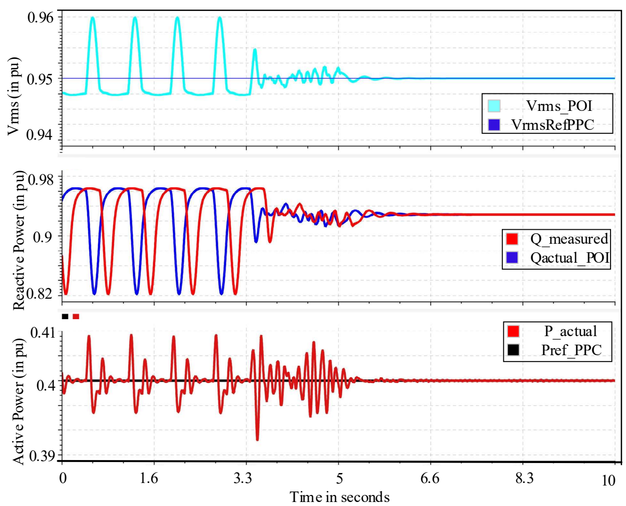

Fig. 9. Delay of 0.25s is added and MLPNN is enabled at 3.3s.

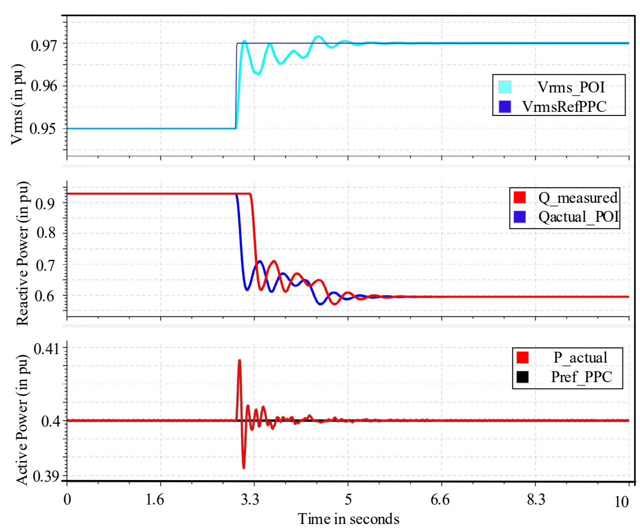

Fig. 10. Vrms step change with 0.25s delay and MLPNN enabled.

979-8-3315-8138-1

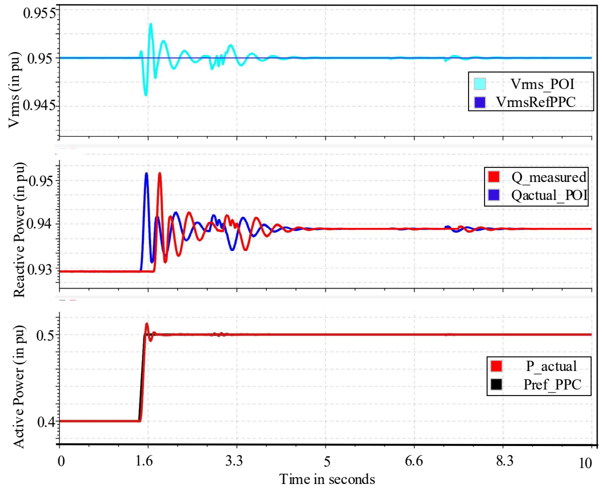

Fig. 11. Reference Pref changed with both delay and MLPNN enabled.

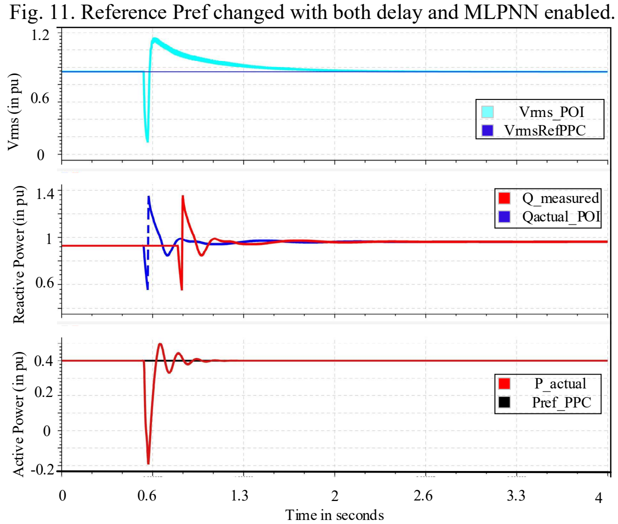

Fig. 12. Fault response at the POI with delay and MLPNN both enabled.

Table 3 presents a qualitative comparison of existing delay compensation methods. The major difference between the classical methods and MLPNN is the required information of the plant. Both the classical methods, Smith predictor [11] and observer-based prediction [12], need the linear model of the plant and as a result, the performance is affected as the plant parameter changes. The computation burden is also high as the plant model has to be computed every time. Weight/gain adaptation is usually not employed in classical methods as they use fixed plant models, while MLPNN updates its weights and thus adapts to parameter drifts.

Table II. Frequency- damping ratio computation with time range

	Time range (MLPNN enabled at 3.3s)					
	0s-3s		**2s-5s**		**2s-7s**	
Case 1	Freq.	Zeta	Freq.	Zeta	Freq.	Zeta
	1.31	0.04	1.26	0.87	1.33	1
Case 2	Freq.	Zeta	Freq.	Zeta	Freq.	Zeta
	1.32	0.02	1.27	1	1.29	1

Table III. Comparison table

Basis	**MLPNN BP**	**Smith Pred.[11]**	**Observer[12]**
Plant model	Not required	Required	Required
Sensitivity to plant model change	Not affected	Affected	Affected
Computation burden	Medium	High	Low
Weight/gain updation	Yes, conditional	No	No

I. Conclusion

This paper proposes a delay-compensation block implemented in the power plant controller (PPC) of a renewable energy system. The proposed block employs a multi-layer perceptron neural network (MLPNN), implemented on a DSP and validated using a real-time digital simulator (RTDS)–based hardware-in-the-loop (HIL) setup. Real-time results indicate that a 0.25-s delay introduces sustained oscillations at approximately 1.33 Hz in reactive power and voltage in the simulated system. With the proposed delay compensation enabled, these oscillations are effectively damped, resulting in improved reactive power and RMS voltage regulation. Frequency-domain analysis reveals a dominant oscillatory mode near 1.3 Hz, whose damping ratio improves from 0.03 to 0.87 and approaches unity after activation of the MLPNN. The proposed approach also demonstrates satisfactory performance during step changes in voltage and active power reference commands and prevents prolonged high-voltage during post-fault recovery after a three-phase fault at the POI.

Further research is ongoing for a technique to compensate variable delays and to mitigate the effect of communication losses between the PQM and the PPC.

References

[1] J. L. Sawin, "Renewables 2020-Global status report," 2010.

[2] S. Jacobsson and A. Johnson, "The diffusion of renewable energy technology: an analytical framework and key issues for research," *Energy Policy*, vol. 28, no. 9, pp. 625–640, Jul. 2000.

[3] F. Porrua, R. Chabar, L. M. Thome, L. A. Barroso, and M. Pereira, "Incorporating large-scale renewable to the transmission grid: Technical and regulatory issues," in *2009 IEEE Power & Energy Society General Meeting*, Calgary, Canada: IEEE, Jul. 2009, pp. 1–7.

[4] A. K. Tiwari, A. Dubey, P. Selvaraj, and S. K. Panda, "Implementation of Active and Reactive Power Control in a Novel Solar Power Plant Controller Solution," in *2021 9th IEEE International Conference on Power Systems (ICPS)*, Kharagpur, India: IEEE, Dec. 2021, pp. 1–6.

[5] A. Kumar, S. Ray, E. Mathew, and A. Gautam, "Impact of Power Plant Controller on Voltage Oscillations in RE complex: Insights from Hardware-in-the-Loop Simulation," in *2025 IEEE Power Energy Society General Meeting (PESGM)*, Austin, USA, Jul. 2025, pp. 1–5.

[6] "Reports on Events Involving Transmission Grid-Connected Wind and Solar Power Plants," Grid Controller of India, 2023.

[7] L. Fan and Z. Miao, "An Explanation of Oscillations Due to Wind Power Plants Weak Grid Interconnection," *IEEE Trans. Sustain. Energy*, vol. 9, no. 1, pp. 488–490, Jan. 2018.

[8] N. Jankovic, J. Roldán-Pérez, M. Prodanovic, and L. Rouco, "Centralised Multimode Power Oscillation Damping Controller for Photovoltaic Plants With Communication Delay Compensation," *IEEE Trans. Energy Convers.*, vol. 39, no. 1, pp. 311–321, Mar. 2024.

[9] J. M. Mauricio, Á. Rodríguez Del Nozal, and A. E. Leon, "A constraint-aware controller for renewable power plant operation under communication delays," *Electric Power Systems Research*, vol. 246, p. 111635, Sep. 2025, doi: 10.1016/j.epsr.2025.111635.

[10] M. Lu, X. Wang, P. C. Loh, F. Blaabjerg, and T. Dragicevic, "Graphical Evaluation of Time-Delay Compensation Techniques for Digitally Controlled Converters," *IEEE Trans. Power Electron.*, vol. 33, no. 3, pp. 2601–2614, Mar. 2018.

[11] T. Nussbaumer, "Comparison of Prediction Techniques to Compensate Time Delays Caused by Digital Control of a Three-Phase Buck-Type PWM Rectifier System," *IEEE Trans. Ind. Electron.*, vol. 55, no. 2, pp. 791–799, 2008.

[12] V. Miskovic, "Observer-based active damping of LCL resonance in grid-connected voltage source converters," in *2013 IEEE Energy Conversion Congress and Exposition*, Denver, USA, Sep. 2013, pp. 4850–4856.

[13] A. Antunes, F. M. Dias, and A. Mota, "A neural network delay compensator for networked control systems," in *2008 IEEE International Conference on Emerging Technologies and Factory Automation*, Hamburg, Germany: IEEE, Sep. 2008, pp. 1271–1276.

979-8-3315-8138-1